AGU100 ADVANCING EARTH AND SPACE SCIENCE

Geophysical Research Letters

RESEARCH LETTER
10.1029/2018GL079293

Key Points:
- We search globally for teleconnections between autumn-lead sea surface salinity (SSS) and winter precipitation in southwestern United States (SWUS)
- SSS can skillfully explain variability in winter precipitation patterns in SWUS
- SSS-based models can outperform traditional SST-based climate indices in predictability of winter SWUS precipitation

Supporting Information:
- Supporting Information S1

Correspondence to:
T. Liu,
tianjialiu@g.harvard.edu

Citation:
Liu, T., Schmitt, R. W., & Li, L. (2018). Global search for autumn-lead sea surface salinity predictors of winter precipitation in southwestern United States. *Geophysical Research Letters*, *45*, 8445–8454. https://doi.org/10.1029/2018GL079293

Received 9 MAR 2018
Accepted 5 AUG 2018
Accepted article online 13 AUG 2018
Published online 22 AUG 2018

©2018. American Geophysical Union. All Rights Reserved.

Global Search for Autumn-Lead Sea Surface Salinity Predictors of Winter Precipitation in Southwestern United States

T. Liu[1,2], R. W. Schmitt[3], and L. Li[4]

[1]Department of Earth and Environmental Sciences, Columbia University, New York, NY, USA, [2]Department of Earth and Planetary Sciences, Harvard University, Cambridge, MA, USA, [3]Department of Physical Oceanography, Woods Hole Oceanographic Institution, Woods Hole, MA, USA, [4]Department of Earth and Ocean Sciences, Nicholas School of the Environment, Duke University, Durham, NC, USA

Abstract Sea surface salinity (SSS) is sensitive to changes in ocean evaporation and precipitation, that is, to changes in the oceanic water cycle. Through the close connection between the oceanic and terrestrial water cycle, SSS can be used as an indicator of rainfall on land. Here we search globally for teleconnections between autumn-lead September-October-November SSS signals and winter December-January-February precipitation over southwestern United States. The SSS-based model (R^2 = 0.61) outperforms the sea surface temperature-based model (R^2 = 0.54). Further, a fresh tropical Pacific in autumn, indicated by low SSS, corresponds with wet winters. Recent studies suggest that anomalously high rainfall in the tropics may excite Rossby waves that can export water to the extratropics. Thus, incorporating SSS, a sensitive indicator of regional oceanic rainfall, can enhance the accuracy of existing precipitation prediction frameworks that rely on sea surface temperature-based climate indices and, by extension, improve watershed management.

Plain Language Summary The global ocean makes up the bulk of the global water cycle and is the ultimate source of all rainfall, implying that changes in the ocean affect rainfall patterns on land. Traditionally, seasonal to decadal sea surface temperature-based patterns have been linked to variations in rainfall over land. However, the salinity of the surface ocean is directly responsive to changes in evaporation and precipitation. We find that abnormally salty (more evaporation) or fresh (more precipitation) patches of the ocean can be used to predict rainfall on land one season ahead. Specifically, we looked globally for changes in autumn sea surface salinity (SSS) that correspond well with variations in winter precipitation in the southwestern United States to build an SSS-based model. We find that the SSS-based model outperforms the sea surface temperature-based model. Thus, incorporating SSS into existing frameworks for predicting seasonal rainfall on land can improve forecasts needed for allocating water resources ahead of abnormally dry or wet seasons.

1. Introduction

The ocean holds 96.5% of total global water and thus plays a key role in the water cycle (Gleick, 1996). The ocean component of the global water cycle, involving 85% of evaporation and 77% of precipitation, dominates the terrestrial component, which only comprises 15% of evaporation and 23% of precipitation (Durack, 2015; Schanze et al., 2010; Schmitt, 1995). It thus follows that the global ocean's evaporation-to-precipitation excess drives ocean-to-land moisture transport and is an indispensable water source for terrestrial precipitation. In this study, we focus on sea surface salinity (SSS) as a tracer of changes in evaporation and precipitation. This relationship can be observed in long-term trends of global SSS and intensification of the water cycle (Durack et al., 2012; Durack & Wijffels, 2010). As global temperatures rise, more evaporation makes salty regions (e.g., subtropical gyres) saltier, and conversely, more precipitation makes fresh regions (e.g., high latitudes and tropics) fresher (Lagerloef et al., 2010). These changes in SSS, and thus the global water cycle, will likely be reflected in the severity and frequency of terrestrial precipitation events (e.g., Cai et al., 2012; Gimeno et al., 2013; Seager et al., 2010). Since evaporation is the primary means by which the ocean supplies water and energy to the atmosphere, we should expect SSS anomalies (SSSAs) to be good indicators of variability in the water cycle. That is, if some part of the ocean becomes saltier than normal, simple mass conservation guarantees that there will be more rainfall somewhere else in the climate system.

Teleconnections have been observed between regional rainfall variability and traditional sea surface temperature (SST)-based climate indices, such as Niño 3.4 (e.g., Gissela et al., 2004; Sharma et al., 2000), Pacific Decadal Oscillation (PDO; e.g., Chan & Zhou, 2005; Krishnamurthy & Krishnamurthy, 2014), and Atlantic Meridional Oscillation (AMO; e.g., Zhang & Delworth, 2006). However, Li et al. (2016a, 2016b) showed that SSS can be a more skillful seasonal terrestrial rainfall predictor than SST-based climate indices. They found that spring Northwest Atlantic SSS leads summer U.S. Midwest rainfall and Northeast Atlantic SSS leads monsoon African Sahel rainfall. Li et al. (2016a, 2016b) explained the teleconnections physically with ocean-to-land moisture transport and local soil moisture feedback mechanisms. Li et al. (2016b) showed that including SSSA into a prediction model almost triples its ability to predict monsoonal precipitation over the African Sahel. Notably, SSSA can be used as a predictor in addition to SSTA, because it is a unique imprint of upstream exchanges between ocean and terrestrial water reservoirs and independent of SSTA's influence on precipitation (Li et al., 2016b).

This study focuses on the predictive skill of global autumn SSS and SST patterns for winter precipitation for the southwestern United States (SWUS). In this region, winter precipitation, especially that stored as snowpack, is necessary for sustaining the water supply through relatively dry summers (Mote et al., 2005). California, in particular, endured a severe multiyear drought that began in 2012 and ended in 2017. In moderate and high carbon emission scenarios, the SWUS will need to adapt to unprecedented risk of decadal to multidecadal droughts in the 21st century (Cook et al., 2015). In the coastal SWUS, two primary factors contribute to increased risk of drought: (1) enhanced interannual precipitation variability due to concomitant declines in daily precipitation and increases in extreme precipitation frequency (Polade et al., 2014; Polade et al., 2017) and (2) enhanced evaporative demand associated with the long-term warming trend (Cayan et al., 2010). The unpredictability of western U.S. droughts in duration and severity on top of the dry SWUS hydroclimate poses policy-making challenges, especially as climate change will likely generate additional strain on agriculture (Lobell et al., 2014), wildfire-prone forests (Westerling et al., 2006), ecosystems (Palmer et al., 2009), hydropower generation (Gleick, 2016), and nonrenewable groundwater reservoirs (Scanlon et al., 2012a; Swain, 2015). Given the disproportionate socioeconomic effect of enhanced drought risk, better drought predictability is important to help policymakers more adequately manage water resources to maintain ecosystem health and support the growing human population (Swain, 2015).

Li et al. (2016a, 2016b) looked globally for terrestrial rainfall teleconnections for North Atlantic SSSAs on a seasonal scale with a 3-month lead time. Here we do the opposite. We search globally for autumn SSS, as well as SST, signals for winter SWUS precipitation, the season when it gets most of its moisture. Our approach is similar to the flexible framework in Gershunov and Cayan (2003), who assessed the predictive skill of SST patterns on seasonal precipitation and identified predictors without a priori assumptions about specific climate modes. We use SWUS as a paradigm to present a framework to quantitatively define and select predictors for building SSS and SST-based models of seasonal terrestrial precipitation.

2. Data and Methods

2.1. Study Region

The study region is the U.S. southwest, which we take to encompass Southern California, Arizona, and western New Mexico (Figure 1a). We define SWUS with a bounding box (southwest corner: 122.75°W, 31.25°N; northeast corner: 105.75°W, 37°N). In the winter months (December through February), this region is relatively dry compared to the rest of the contiguous United States. We assume uniform spatial variability within the study region due to strong correlation ($R = 0.77 \pm 0.12$) of gridded winter precipitation within the defined boundaries of SWUS (Figure S1 in the supporting information).

2.2. Data Sets

The U.S. precipitation data set used in this study is the National Oceanic and Atmospheric Administration (NOAA) Climate Prediction Center (CPC) unified gridded gauge-based data set (0.25° × 0.25° spatial resolution, daily, 1948–2018; Higgins et al., 2000; https://esrl.noaa.gov/psd/data/gridded/data.unified.daily.conus.html). The temporal range of this study is limited by the availability of the CPC Unified data set; we study 70 years of data that spans 1948–2018.

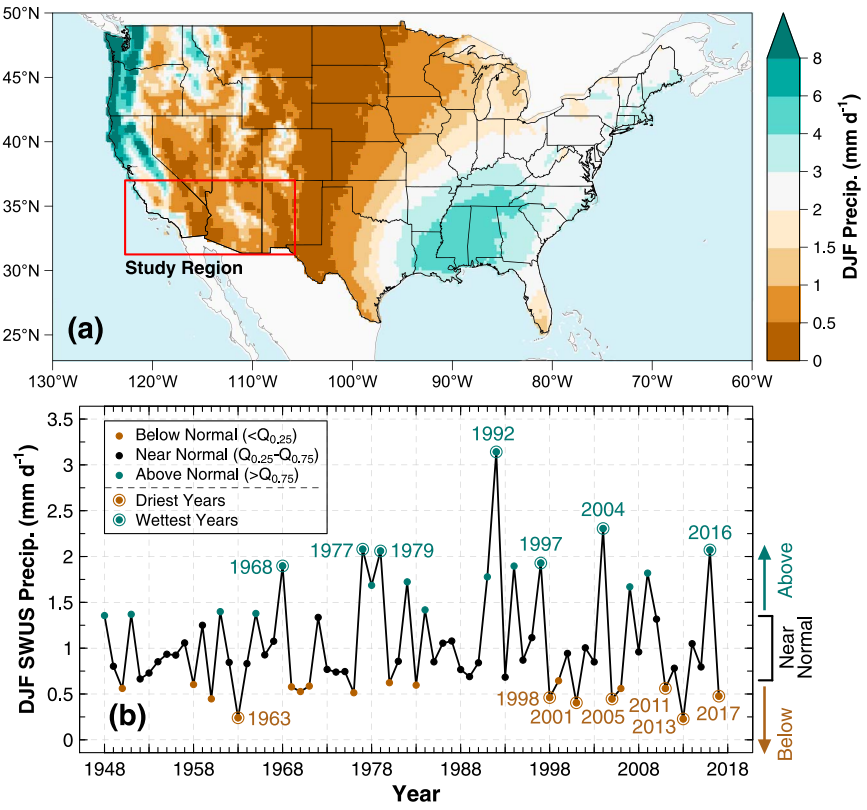

Figure 1. Winter precipitation in southwestern United States (SWUS). (a) Winter (December-January-February) precipitation in the contiguous United States. The study region, SWUS, is defined by the red box. (b) SWUS winter precipitation, averaged temporally across days from December to February and spatially within grid cells in the study region, over 1948–1949 to 2016–2018. The 7 wettest years (top decile) and 7 driest years (bottom decile), after detrending, are denoted as circled green and brown dots, respectively.

The ocean salinity and temperature data sets used in this study are from the United Kingdom Met Office Hadley Centre EN4.2.1 (1° × 1° spatial resolution, monthly, 1900–2017) quality-controlled objective analyses data set with Gouretski and Reseghetti (2010) bias corrections applied (Good et al., 2013; https://www.metoffice.gov.uk/hadobs/en4/). EN4.2.1 mainly uses observational data from the World Ocean Database 2013, Global Temperature and Salinity Profile Project (from 1990), and Argo float data (from 2000). We use the monthly salinity and temperature observations at 0–10 m depth as SSS and SST, respectively, averaged from September to November.

The traditional SST-based climate indices considered in this study are Niño 1 + 2, Niño 3, Niño 3.4, Niño 4, AMO, and PDO (Table S1 in the supporting information; Rayner et al., 2003; Mantua et al., 1997; Zhang et al., 1997; Enfield et al., 2001). Data are from the NOAA Earth System Research Laboratory Physical Sciences Division (https://www.esrl.noaa.gov/psd/gcos_wgsp/Timeseries/).

2.3. Statistical Methods

We construct a detrended time series for winter (December-January-February, DJF) precipitation, averaged over SWUS (Figure 1b). The variability of regional winter SWUS precipitation most closely reflects that of local winter precipitation in Southern California and western-central Arizona. We further categorize precipitation as follows: near normal (25th to 75th percentile: 0.67–1.36 mm d^{-1}), below normal (<25th percentile), and above normal (>75th percentile; Figure 1b).

We detrend precipitation, SSS, and SST time series to prevent autocorrelation and isolate teleconnection patterns between predictors and predictand that are more likely to be physically meaningful. That is, we focus on the variance of signals rather than trends in global oceanic predictors and regional precipitation.

First, we broadly characterize the strongest signals in autumn (September-October-November) SSSA and SSTA for the wettest and driest years: The top and bottom deciles of the 70-year winter SWUS precipitation record (7 years) represent high (wet) and low (dry) precipitation cases, respectively. We run 1,000 iterations of the Monte Carlo simulation (Livezey & Chen, 1983) to test the significance level of the SSSA and SSTA composites. We define statistical significance as $p < 0.05$.

We then use statistical modeling to explore the 70-year precipitation record in-depth. First, we estimate the correlation coefficient (R) for the detrended SSS (SST) and winter precipitation time series on a pixel-by-pixel basis. Co-location of highly correlative areas with SSS and SST signals from the wet and dry case composites supports linearity and relative stationarity of such signals. To isolate the strongest linear signals, we exclude high latitudes (above 60°N and below 60°S) due to highly variable ocean temperature and salinity in the polar regions and the relative lack of observations in the Southern Ocean. We then filter grid boxes with two thresholds: a correlation threshold, T_1, and an area threshold, T_2. Adjoining pixels with $|R| > T_1$ threshold are aggregated to form polygons. We filter out weak correlation areas that have little potential to be skillful predictors and consider $0.2 \leq T_1 \leq 0.25$ at intervals of 0.01. We further assume low confidence in smaller polygons, which may be products of statistical noise. Thus, we filter out polygons with areas smaller than 50 pixels (~6×10^5 km^2 at equator): $T_2 = 50$. Physically, anomalous signals larger than a spatial scale of 10^3 km^2 are more likely to generate persistent climate impact (Sawyer, 1965). The remaining polygons are used to extract and average autumn SSS (SST) in order to form independent time series that serve as predictors in the multivariate linear regression models. We assess the temporal stability in the strength of the isolated signals with 30-year running correlations.

We use the *regsubsets* function in the R leaps package to perform best subset regression (Lumley, T. based on Fortran code by Alan Miller, 2017). Prior to regression analysis, we remove the linear trend from the data and check for extreme multiple collinearity, removing variables with a variance inflation factor greater than 4. We use multivariate linear regression with regulation to select the best combination of autumn SSS (SST) predictors of winter SWUS precipitation among 8 "best" models spanning 1–8 total predictors. To objectively select the final model and prevent overfitting, we use the Bayesian information criterion (BIC), a metric with a higher penalty term compared to the Akaike information criterion; BIC prefers simpler models, or inclusion of fewer predictors (Schwarz, 1978). The model with the lowest BIC is selected.

To further test model performance, we use the repeated hold-out method. We split the 70-year SSS (SST) and precipitation data into training and test data sets. That is, we train the models on two thirds (47 years) of the SSS (SST) and precipitation data sets to predict the other one third (23 years) of data. We repeat this process for holding out half the years for the test data set. For 1,000 iterations, we randomly subsample the years of data used for the training and test data sets and obtain the variance explained (adjusted R^2) in the test data set. To further test model predictive skill, we simulate "seasonal outlooks" for the following winter's precipitation by retraining the SSS and SST-based models on "historical" data from all years prior. More specifically, we generate 67-, 68-, and 69-year SSS and SST models to predict the near-normal, above-normal, and below-normal precipitation in winter 2015–2016, 2016–2017, and 2017–2018 respectively.

3. Beyond Climate Indices: Global Search for SSS Teleconnections

The autumn-lead SST-based traditional climate indices are not skillful (adjusted $R^2 = 0.03$–0.06) in the prediction of winter SWUS precipitation (Table S1). For example, the most skillful SST-based index, Niño 3.4, can only explain 6% of variance in winter SWUS precipitation. This low skill may be explained by the inherent instability and nonstationary nature of climate teleconnections (e.g., Gershunov et al., 2001), as manifested in the lack of ENSO-driven variability in winter precipitation over SWUS in the 21st century. For 30-year increments, the skill of ENSO-related climate indices peaked around 1970–2010 and has since continued to decrease. Another possibility is the increasing frequency of other flavors of El Niño, namely, central Pacific El Niño (El Niño Modoki; Paek et al., 2017). In this secondary mode of El Niño, the eastern Pacific is cool, while the central Pacific is warm (Ashok et al., 2007).

As expected, the SSTA signal is dominated by the El-Niño–Southern Oscillation (ENSO; Figures 2c and 2d). When SWUS experiences anomalously wet winters, a strong dipole of cool water in the western Pacific Ocean and a warm tongue extending from the central to eastern equatorial Pacific is present in the

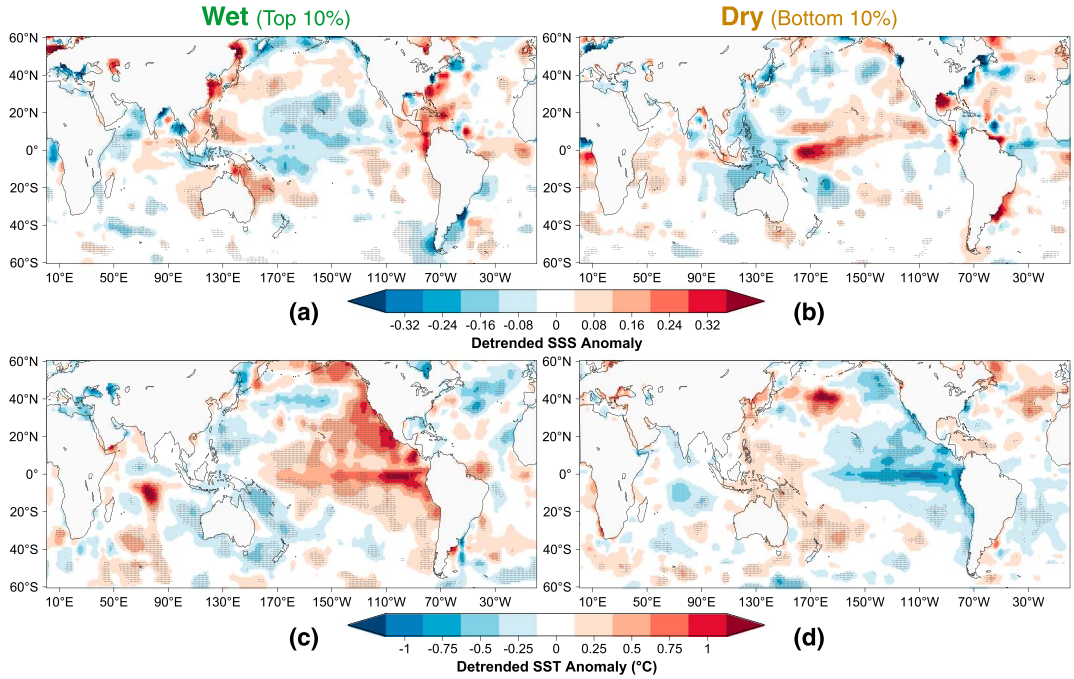

Figure 2. Sea surface salinity anomaly (SSSA) and sea surface temperature anomaly (SSTA) composites for dry and wet winters. Detrended autumn (a and b) SSSA and (c and d) SSTA composites for the wet and dry deciles of winter southwestern United States precipitation. The stippled grid boxes represent statistical significance ($p < 0.05$) based on 1,000 Monte Carlo simulations.

preceding autumn. The warm tongue is coupled with the Pacific Warm Blob, which is characteristic of warm waters along the western coast of North America and linked to the strong 2015–2016 El Niño event (Tseng et al., 2017). The SSS signal is likely linked to ENSO. The warm-cool dipole center is co-located with a fresh central-western equatorial Pacific (Figure 2a). During El Niño, freshwaters are advected westward and precipitation excess further contributes to this western fresh pool (Delcroix & McPhaden, 2002; Picaut et al., 1996). Conversely, the La Niña mode cool-warm dipole center is co-located with a salty central-western equatorial Pacific (Figure 2b).

Similar spatial patterns in the wet and dry case composites as in the highly correlative patches confirm the linearity of strong SSS and SST signals in the tropics with SWUS precipitation (Figures 2, 3a, and 3c). The SSS correlation map shows that a fresh tropical Pacific precedes wet winters in SWUS (Figure 3a). The SST correlation map shows that a dipole pattern of a warm central-east tropical Pacific and cool central-west tropical Pacific precedes wet winters in SWUS (Figure 3c). We identify and isolate 19 potential SSS predictors and 12 potential SST predictors, respectively (Tables S2 and S3). All predictors are correlated with winter SWUS precipitation at $p < 0.05$. Small standard deviations in the 30-year running correlations between SSS and SST predictors and winter SWUS precipitation suggest that many SSS and SST teleconnections are relatively stable (Tables S2 and S3). However, linear trends in these correlations show some instability in strong teleconnection patterns whose skill is increasing (many SSS predictors, e.g., SSS8 and SSS12) or decreasing (many SST predictors, e.g., SST9 and SST10) with time.

Many of the identified SSS and SST predictors are linked to the SST-based climate indices, particularly to ENSO (Tables S6 and S7). We emphasize that almost all the identified SSS and SST predictors are individually more skillful than the traditional climate indices: for example, central tropical Pacific SSS (SSS18, $R = -0.38$), western tropical Pacific SST (SST1, $R = -0.51$), central tropical Pacific SST (SST9, $R = 0.37$), and northeastern Pacific SST (SST12, $R = 0.46$; Tables S2 and S3). This suggests that more flexible, region-specific definitions of SST indices can greatly improve precipitation forecasts. For example, using SST1 (adjusted $R^2 = 0.25$) rather than Niño 3.4 (adjusted $R^2 = 0.06$) more than quadruples the variance explained in winter SWUS precipitation (Figure 3c and Tables S1 and S3).

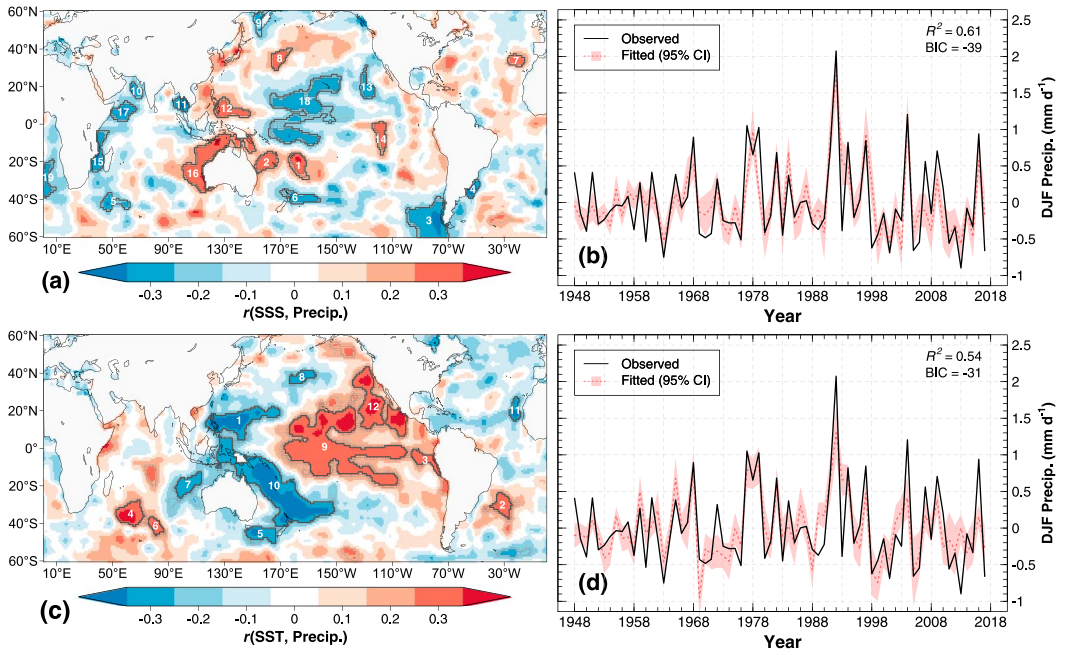

Figure 3. Global sea surface salinity (SSS) and sea surface temperature (SST)-based "best" models of winter southwestern United States (SWUS) precipitation. (a) Pixel-by-pixel correlation of detrended autumn (a) SSS and (c) SST with winter SWUS precipitation, with identified predictors bounded in black. (b) The SSS multivariate linear regression model, using seven predictors (SSS4, 7, 8, 10, 11, 12, and 19), explains 61% of variance in winter precipitation. (d) The SST multivariate linear regression model, using six predictors (SST1, 2, 5, 6, 7, and 11), explains 54% of variance in winter precipitation.

The SSS model (adjusted R^2 = 0.61, BIC = −39) is more skillful than the SST model (adjusted R^2 = 0.54, BIC = −31; Figure 3 and Table S4). The mean variances of the test data sets explained by SSS and SST training models is 51–53% and 46–47%, respectively, using the repeated hold-out method (Table S5). That is, using two thirds to half the years of EN4 data, we are able to more skillfully predict the other one third to half of precipitation data using SSS rather than SST. Unlike the SSS model, the SST model is unable to resolve the dry 2013–2014 and wet 2016–2017 winters. Moreover, in terms of predictive skill for the 2015–2016 and 2016–2017 winters, the SSS model outperforms the SST model (Table S8). The September–November issues of the CPC Seasonal Outlook for DJF 2015–2016 and 2016–2017 are mostly consistent with the SST model (CPC, 2015, 2016). For winter 2015–2016, the SST model (1.65 mm d^{-1}, relative error: +107%) overpredicts while the SSS model (0.96 mm d^{-1}, relative error: +21%) accurately estimates the near-normal winter mean daily precipitation (0.79 mm d^{-1}). Similarly, the SSS model (1.38 mm d^{-1}, relative error: −33%) outperforms the SST model (0.67 mm d^{-1}, relative error: −68%) in predicting the above-average daily precipitation (2.07 mm d^{-1}) in winter 2016–2017. However, both models overpredict the abnormally dry 2017–2018 winter (0.48 mm d^{-1}) by 179–204%, in contrast to the more accurate CPC Seasonal Outlook for DJF 2017–2018 (CPC, 2017).

4. Potential Mechanisms for Long-Range Moisture Transport

Rossby waves are large, high-altitude, meandering atmospheric wind patterns that can transport moisture from the tropics to the extratropics (Rossby, 1940; Hoskins & Karoly, 1981). The heat applied to the atmosphere from anomalous tropical rainfall can generate standing Rossby waves that propagate to high latitudes. In particular, the tropical Pacific is a major "hot spot" for exciting seasonal Rossby waves that propagate to the subtropics (Scaife et al., 2017). Molteni et al. (2015) suggest that tropical rainfall is a more direct driver of teleconnections than SST. Since rainfall contributes much more of the variance in SSS than evaporation (Zeng et al., 2018), this may well explain our finding that remote SSS variations have greater utility in predicting extratropical rainfall than SST. Covariance patterns found in Molteni et al. (2015) reveal teleconnections between tropical Pacific and terrestrial rainfall

anomalies that propagate across the SWUS. Indeed, the teleconnection hot spots in eastern and central tropical Pacific are consistent with the spatial distribution of highly correlative areas between autumn SSS and winter SWUS precipitation (Figures 2 and 3). Thus, the anomalous fresh region that we observe in the tropical Pacific preceding wet winters in SWUS may indicate an active winter, wherein excited standing Rossby waves transport higher-than-usual moisture from the tropics to SWUS (Figures 2a and 3a).

Scaife et al. (2017) find that seasonal Rossby waves do not vary in position but do vary in activity across winters depending on tropical rainfall anomalies. Additionally, Branstator and Teng (2017) find that jets, which act as waveguides for Rossby wave propagation, are circumglobal in the winter but confined to certain regions during the summer. Indeed, Jiménez-Esteve and Domeisen (2018) conclude that the stratosphere can modulate transient Rossby wave propagation across North America during the winter, therefore bridging Pacific and North Atlantic through the troposphere. Hu et al. (2017) found a connection between large-scale Rossby wave breaking and atmospheric rivers (ARs) making landfall on U.S. West Coast. Even though the 2016–2017 winter is not associated with a strong El Niño like the previous winter, "Pineapple Express" ARs lifted California out of its multiyear drought (Gershunov et al., 2017). ARs are long, narrow, and filamentary corridors that can export large amounts of water from the tropics to the extratropics (e.g., Zhu & Newell, 1998). The Pineapple Express, a particular type of AR, transports moisture from the Hawaii region to California (e.g., Dettinger, 2004; Dettinger, 2015; Dettinger et al., 2011). However, the ARs that affect the coastal regions differ from those that propagate to Arizona (Gershunov et al., 2017; Rutz et al., 2014), underscoring the inconsistency of AR impact across the SWUS domain. Taken together, recent studies (e.g., Branstator & Teng, 2017; Hu et al., 2017; Molteni et al., 2015; Rutz & Steenburgh, 2012; Scaife et al., 2017) suggest that more accurate prediction of Rossby waves, as well as AR events, may increase the predictability of winter precipitation in SWUS.

Increasing SSSA variability over the central tropical North Pacific over the past few decades suggests amplification of the SSS signal (Figure S2). Critically, the recent see-saw from extreme drought to flooding in California and its unpredictability is a challenge for making decisions on allocation of water management resources and likely a precedent for similar drought-to-flood events in the future (Diffenbaugh et al., 2015; Shields & Kiehl, 2016; Wang et al., 2017). In particular, the abnormally saline phase of the tropical Pacific, which may have subdued the export of water to the subtropics during the recent drought years, is followed by a rapid turnover to an abnormally fresh phase during the 2015–2016 El Niño, persisting to the wet 2016–2017 winter. However, atmospheric patterns can complicate the SSS teleconnections. Presence of an atmospheric ridge along the U.S. West Coast, even if commensurate with low tropical Pacific SSS, may divert storm tracks northward such as during the dry 2012–2015 winters (Swain et al., 2016; Teng & Branstator, 2016; Figure S4). For example, in contrast to the strong atmospheric trough over the U.S. West Coast in late 2016, its absence in 2015 may be responsible for the drier-than-usual SWUS winter despite expansive fresh pools in the tropical Pacific (Figures S5a and S5b). Rather, the atmospheric trough located offshore in the Northeast Pacific in autumn 2015 may have displaced potential ENSO-enhanced rainfall offshore as seen in the extreme oceanic and coastal forcing in winter 2015–2016 (Figure S5a; Barnard et al., 2017).

Additionally, SSS variability in the central equatorial Pacific is not as strongly linked to ENSO as SST variability (Chen et al., 2012; Di Lorenzo et al., 2005; Tables S6 and S7), such as seen in autumn 2016 relative to 2015 (Figures S3a–S3d). Despite the retreat of the 2015–2016 strong El Niño, fresh pools in the central-eastern and western tropical Pacific were still present in autumn 2016 (Figure S3c). Aside from the apparent recent amplification in SSS signals in the tropical Pacific, we observe approximately 12-year SSSA cycles in the central tropical-subtropical North Pacific from 1991–2003 and 2003–2015, with the latter cycle more pronounced in terms of amplitude (Figure S2). In each case, SSS in the North Pacific slowly increased before decreasing to a local minimum. Chen et al. (2014) linked decadal SSS variability to the North Pacific Gyre Oscillation (NPGO), a low-frequency decadal SSS mode attributed to global climate variability (Di Lorenzo et al., 2009, 2010). However, we find only moderate agreement between SSS18 and NPGO ($R = 0.54$, $p < 0.05$; Figure S2), on par with PDO ($R = -0.52$, $p < 0.05$) and ENSO ($R = -0.5$ to -0.57, $p < 0.05$; Table S6). Unlike SSS18, we find that autumn NPGO is a poor predictor of winter SWUS precipitation (adjusted $R^2 = 0.02$, $p = 0.14$), again signaling a need to search for skillful predictors beyond traditional climate indices.

5. Future Directions

Notably, the regional setting for predictive models of terrestrial rainfall is not confined to SWUS and can be extended to any geographic or administrative boundaries, such as climate divisions and watershed delineations. For example, by scaling up the analysis, we can investigate how SSSA and SSTA teleconnection patterns and predictability of rainfall spatially vary by subregional watersheds, as defined by the United States Geological Survey, within the SWUS. Further, global and local precipitation data sets can be substituted for the Palmer Drought Severity Index to focus on agriculture, historical terrestrial rainfall and temperature, and soil moisture content, for example (Dai et al., 2004). SSS and SST predictors can also be individually optimized with different lead times; for example, Mamalakis et al. (2018) show that observations of long-lead late summer SST in the southwestern Pacific, a teleconnection modulated through a western Pacific atmospheric bridge pathway, can enhance predictability of winter SWUS precipitation. Further, SSS and SST uncertainty estimates and adjustments in correlation thresholds can be used to fine-tune the predictive models and generate ensemble predictions. Lastly, more extensive analysis on SSS with regard to moisture flux divergence, latent heat flux, ocean circulation, and geopotential height may help to pinpoint dynamic and thermodynamic mechanisms for isolated SSS-precipitation teleconnections and decouple myriad oceanic-atmospheric contributors to variability in regional precipitation.

6. Conclusions

In our preliminary analysis, we present a simple method to globally search for and isolate teleconnections between autumn-lead SSS and SST and winter SWUS precipitation. First, we use pixel-by-pixel correlations between the detrended autumn SSS and SST and winter SWUS precipitation time series to identify and define potential predictors. We then use multivariate linear regression with regulation (best subset regression and BIC) to objectively select the best models using SSS and SST predictors. In the case of the SWUS, the SSS model (R^2 = 0.61) outperforms the SST model (R^2 = 0.54). SSS and SST models can more skillfully explain the variance in winter SWUS precipitation than traditional SST-based climate indices (Niño 1 + 2, Niño 3, Niño 3.4, Niño 4, PDO, and AMO), which only explain 3–6% of variance. As a complement to SST, SSS is an indicator of the export of water and latent heat from ocean to atmosphere and responds to wind-driven advection and mixing (Lagerloef et al., 2010; Schmitt, 1995). Thus, it is sensitive to air-sea exchanges that have surprising long-range predictive utility for terrestrial rainfall. We hypothesize that low SSS in the tropical Pacific indicates anomalous rainfall that can excite Rossby waves, thereby providing a channel to export water from the tropics to the extratropics. Thus, we find that SSS, as measured by the ARGO float array and salinity satellites SMOS and SMAP, is a useful climate variable that can significantly improve predictions of seasonal precipitation variability on land.

Acknowledgments

T. Liu was supported by a Woods Hole Oceanographic Institution Summer Student Fellowship and NSF Graduate Research Fellowship (DGE1144152 and DGE1745303). R. Schmitt was supported by NSF grant ICER-1663704. L. Li was supported by NSF grant ICER-1663138. All data used in this study are publicly available. EN4 salinity and temperature data are available from the UK Met Office at https://www.metoffice.gov.uk/hadobs/en4/. The CPC Unified Gauge-based Analysis of Daily Precipitation over contiguous United States and climate index data sets are provided by NOAA/OAR/Earth System Research Laboratory Physical Sciences Division, Boulder, Colorado, USA at https://www.esrl.noaa.gov/psd/.

References

Ashok, K., Behera, S. K., Rao, S. A., Weng, H., & Yamagata, T. (2007). El Niño Modoki and its possible teleconnection. *Journal of Geophysical Research*, *112*, C11007. https://doi.org/10.1029/2006JC003798

Barnard, P. L., Hoover, D., Hubbard, D. M., Snyder, A., Ludka, B. C., Allan, J., et al. (2017). Extreme oceanographic forcing and coastal response due to the 2015–2016 El Niño. *Nature Communications*, *8*, 14,365. https://doi.org/10.1038/ncomms14365

Branstator, G., & Teng, H. (2017). Tropospheric waveguide teleconnections and their seasonality. *Journal of the Atmospheric Sciences*, *74*(5), 1513–1532. https://doi.org/10.1175/JAS-D-16-0305.1

Cai, W., Cowan, T., & Thatcher, M. (2012). Rainfall reductions over Southern Hemisphere semi-arid regions: The role of subtropical dry zone expansion. *Scientific Reports*, *2*(1), 702. https://doi.org/10.1038/srep00702

Cayan, D. R., Das, T., Pierce, D. W., Barnett, T. P., Tyree, M., & Gershunov, A. (2010). Future dryness in the southwest US and the hydrology of the early 21st century drought. *Proceedings of the National Academy of Sciences of the United States of America*, *107*(50), 21,271–21,276. https://doi.org/10.1073/pnas.0912391107

Chan, J. C. L., & Zhou, W. (2005). PDO, ENSO and the early summer monsoon rainfall over South China. *Geophysical Research Letters*, *32*, L08810. https://doi.org/10.1029/2004GL022015

Chen, J., Zhang, R., Wang, H., An, Y., Peng, P., & Zhang, W. (2012). Isolation of sea surface salinity maps on various timescales in the tropical Pacific Ocean. *Journal of Oceanography*, *68*(5), 687–701. https://doi.org/10.1007/s10872-012-0126-8

Chen, J., Zhang, R., Wang, H., Li, J., Hong, M., & Li, X. (2014). Decadal modes of sea surface salinity and the water cycle in the tropical Pacific Ocean: The anomalous late 1990s. *Deep-Sea Research Part I: Oceanographic Research Papers*, *84*, 38–49. https://doi.org/10.1016/j.dsr.2013.10.005

Climate Prediction Center (2015). Monthly and seasonal forecast archives: September, October, November 2015. National Oceanic and Atmospheric Administration. http://www.cpc.ncep.noaa.gov/products/archives/long_lead/llarc.ind.php. Accessed 12 January 2018.

Climate Prediction Center (2016). Monthly and seasonal forecast archives: September, October, November 2016. National Oceanic and Atmospheric Administration. http://www.cpc.ncep.noaa.gov/products/archives/long_lead/llarc.ind.php. Accessed 12 January 2018.

Climate Prediction Center (2017). Monthly and seasonal forecast archives: September, October, November 2017. National Oceanic and Atmospheric Administration. http://www.cpc.ncep.noaa.gov/products/archives/long_lead/llarc.ind.php. Accessed 10 June 2018.

Cook, B. I., Ault, T. R., & Smerdon, J. E. (2015). Unprecedented 21st-century drought risk in the American Southwest and Central Plains. *Science Advances*, *1*(1), e1400082. https://doi.org/10.1126/sciadv.1400082

Dai, A., Trenberth, K. E., & Qian, T. (2004). A global data set of Palmer Drought Severity Index for 1870–2002: Relationship with soil moisture and effects of surface warming. *Journal of Hydrometeorology*, *5*(6), 1117–1130. https://doi.org/10.1175/JHM-386.1

Delcroix, T., & McPhaden, M. (2002). Interannual sea surface salinity and temperature changes in the western Pacific warm pool during 1992–2000. *Journal of Geophysical Research*, *107*, 8002. https://doi.org/10.1029/2001JC000862

Dettinger, M. (2015). Sturm und Drang-California's remarkable storm-drought connection. *Hydrolink*, *1*, 21–22.

Dettinger, M. D. (2004). Fifty-two years of pineapple-express storms across the west coast of North America. California Energy Commission PIER Energy-Related Environmental Research Report CEC-500-2005-004, Sacramento, California, 15 pp.

Dettinger, M. D., Ralph, F. M., Das, T., Neiman, P. J., & Cayan, D. R. (2011). Atmospheric rivers, floods and the water resources of California. *Watermark*, *3*(2), 445–478. https://doi.org/10.3390/w3020445

Di Lorenzo, E., Cobb, K., Furtado, J., Schneider, N., Anderson, B., Bracco, A., et al. (2010). Central Pacific El Niño and decadal climate change in the North Pacific Ocean. *Nature Geoscience*, *3*(11), 762–765. https://doi.org/10.1038/ngeo984

Di Lorenzo, E., Fiechter, J., Schneider, N., Bracco, A., Miller, A., Franks, P., et al. (2009). Nutrient and salinity decadal variations in the central and eastern North Pacific. *Geophysical Research Letters*, *36*, L14601. https://doi.org/10.1029/2009GL038261

Di Lorenzo, E., Miller, A. J., Schneider, N., & McWilliams, J. C. (2005). The warming of the California current system: Dynamics and ecosystem implications. *Journal of Physical Oceanography*, *35*(3), 336–362. https://doi.org/10.1175/JPO-2690.1

Diffenbaugh, N. S., Swain, D. L., & Touma, D. (2015). Anthropogenic warming has increased drought risk in California. *Proceedings of the National Academy of Sciences of the United States of America*, *112*(13), 3931–3936. https://doi.org/10.1073/pnas.1422385112

Durack, P. J. (2015). Ocean salinity and the global water cycle. *Oceanography*, *28*(1), 20–31. https://doi.org/10.5670/oceanog.2015.03

Durack, P. J., & Wijffels, S. E. (2010). Fifty year trends in global ocean salinities and their relationship to broad-scale warming. *Journal of Climate*, *23*(16), 4342–4362. https://doi.org/10.1175/2010JCLI3377.1

Durack, P. J., Wijffels, S. E., & Matear, R. J. (2012). Ocean salinities reveal strong global water cycle intensification during 1950 to 2000. *Science*, *336*(6080), 455–458. https://doi.org/10.1126/science.1212222

Enfield, D. B., Mestas-Nunez, A. M., & Trimble, P. J. (2001). The Atlantic Multidecadal Oscillation and its relation to rainfall and river flows in the continental U.S. *Geophysical Research Letters*, *28*(10), 2077–2080. https://doi.org/10.1029/2000GL012745

Gershunov, A., & Cayan, D. (2003). Heavy daily precipitation frequency over the contiguous United States: Sources of climatic variability and seasonal predictability. *Journal of Climate*, *16*(16), 2752–2765. https://doi.org/10.1175/1520-0442(2003)016<2752:HDPFOT>2.0.CO;2

Gershunov, A., Schneider, N., & Barnett, T. (2001). Low frequency modulation of the ENSO-Indian monsoon rainfall relationship: Signal or noise. *Journal of Climate*, *14*(11), 2486–2492. https://doi.org/10.1175/1520-0442(2001)014<2486:LFMOTE>2.0.CO;2

Gershunov, A., Shulgina, T. M., Ralph, F. M., Lavers, D., & Rutz, J. J. (2017). Assessing climate-scale variability of atmospheric rivers affecting western North America. *Geophysical Research Letters*, *44*, 7900–7908. https://doi.org/10.1002/2017GL074175

Gimeno, L., Nieto, R., Drumond, R., Castillo, R., & Trigo, R. (2013). Influence of the intensification of the major oceanic moisture sources on continental precipitation. *Geophysical Research Letters*, *40*, 1443–1450. https://doi.org/10.1002/grl.50338

Gissela, T., Black, E., Grimes, D. I. F., & Slingo, J. M. (2004). Seasonal forecasting of the Ethiopian summer rains. *International Journal of Climatology*, *24*(11), 1345–1358. https://doi.org/10.1002/joc.1078

Gleick, P. H. (1996). Water resources. In S. H. Schneider (Ed.), *Encyclopedia of climate and weather* (Vol. 2, pp. 817–823). New York: Oxford University Press.

Gleick, P. H. (2016). Impacts of California's ongoing drought: Hydroelectricity generation 2015 update. Pacific Institute.

Good, S. A., Martin, M. J., & Rayner, N. A. (2013). EN4: Quality controlled ocean temperature and salinity profiles and monthly objective analyses with uncertainty estimates. *Journal of Geophysical Research: Oceans*, *118*, 6704–6716. https://doi.org/110.1002/2013JC009067

Gouretski, V., & Reseghetti, F. (2010). On depth and temperature biases in bathythermograph data: Development of a new correction scheme based on analysis of a global ocean database. *Deep-Sea Research Part I*, *57*(6), 812–833. https://doi.org/10.1016/j.dsr.2010.03.011

Higgins, R. W., Shi, W., Yarosh, E., & Joyce, R. (2000). Improved United States precipitation quality control system and analysis (NCEP/Climate Prediction Center ATLAS no. 7).

Hoskins, B. J., & Karoly, D. J. (1981). The steady linear response of a spherical atmosphere to thermal and orographic forcing. *Journal of the Atmospheric Sciences*, *38*, 1179–1196. https://doi.org/10.1175/1520-0469(1981)038<1179:TSLROA>2.0.CO;2

Hu, H., Dominguez, F., Wang, Z., Lavers, D. A., Zhang, G., & Ralph, F. M. (2017). Linking atmospheric river hydrological impacts on the U.S. west coast to Rossby wave breaking. *Journal of Climate*, *30*(9), 3381–3399. https://doi.org/10.1175/JCLI-D-16-0386.1

Jiménez-Esteve, B., & Domeisen, D. I. V. (2018). The tropospheric pathway of the ENSO-North Atlantic teleconnection. *Journal of Climate*, *31*(11), 4563–4584. https://doi.org/10.1175/JCLI-D-17-0716.1

Krishnamurthy, L., & Krishnamurthy, V. (2014). Influence of PDO on South Asian summer monsoon and monsoon-ENSO relation. *Climate Dynamics*, *9-10*, 2397–2410.

Lagerloef, G., Schmitt, R. W., Schanze, J., & Kao, H.-Y. (2010). The ocean and the global water cycle. *Oceanography*, *30*, 82–93.

Li, L., Schmitt, R. W., Ummenhofer, C. C., & Karnauskas, K. B. (2016a). Implications of North Atlantic sea surface salinity for summer precipitation over the U.S. Midwest: Mechanisms and predictive value. *Journal of Climate*, *29*(9), 3143–3159. https://doi.org/10.1175/JCLI-D-15-0520.1

Li, L., Schmitt, R. W., Ummenhofer, C. C., & Karnauskas, K. B. (2016b). North Atlantic salinity as a predictor of Sahel precipitation. *Science Advances*, *2*, 5e1501588.

Livezey, R. E., & Chen, W. Y. (1983). Statistical field significance and its determination by Monte Carlo techniques. *Monthly Weather Review*, *111*(1), 46–59. https://doi.org/10.1175/1520-0493(1983)111<0046:SFSAID>2.0.CO;2

Lobell, D. B., Roberts, M. J., Schlenker, W., Braun, N., Little, B. B., Rejesus, R. M., & Hammer, G. L. (2014). Greater sensitivity to drought accompanies maize yield increase in the U.S. Midwest. *Science*, *344*(6183), 516–519. https://doi.org/10.1126/science.1251423

Lumley, T. based on Fortran code by Alan Miller (2017). leaps: Regression Subset Selection. R package version 3.0. Retrieved from https://CRAN.R-project.org/package=leaps

Mamalakis, A., Yu, J., Randerson, J. T., AghaKouchak, A., & Foufoula-Georgiou, E. (2018). A new interhemispheric teleconnection increases predictability of winter precipitation in southwestern US. *Nature Communications*, *9*(1), 2332. https://doi.org/10.1038/s41467-018-04722-7

Mantua, N. J., Hare, S. R., Zhang, Y., Wallace, J. M., & Francis, R. C. (1997). A Pacific interdecadal climate oscillation with impacts on salmon production. *Bulletin of the American Meteorological Society*, *78*(6), 1069–1079. https://doi.org/10.1175/1520-0477(1997)078<1069:APICOW>2.0.CO;2

Molteni, F., Stockdale, T. N., & Vitart, F. (2015). Understanding and modelling extra-tropical teleconnections with the Indo-Pacific region during the northern winter. *Climate Dynamics*, *45*(11-12), 3119–3140. https://doi.org/10.1007/s00382-015-2528-y

Mote, P. W., Hamlet, A. F., Clark, M. P., & Lettenmaier, D. P. (2005). Declining mountain snowpack in western North America. *Bulletin of the American Meteorological Society*, *86*(1), 39–50. https://doi.org/10.1175/BAMS-86-1-39

Paek, H., Yu, J.-Y., & Qian, C. (2017). Why were the 2015/2016 and 1997/1998 extreme El Niños different? *Geophysical Research Letters*, *44*, 1848–1856. https://doi.org/10.1002/2016GL071515

Palmer, M. A., Lettenmaier, D. P., Poff, N. L., Postel, S. L., Richter, B., & Warner, R. (2009). Climate change and river ecosystems: Protection and adaptation options. *Environmental Management*, *44*(6), 1053–1068. https://doi.org/10.1007/s00267-009-9329-1

Picaut, J., Ioualalen, M., Menkes, C., Delcroix, T., & McPhaden, M. (1996). Mechanism of the zonal displacements of the Pacific warm pool, implications for ENSO. *Science*, *274*(5292), 1486–1489. https://doi.org/10.1126/science.274.5292.1486

Polade, S. D., Gershunov, A., Cayan, D. R., Dettinger, M. D., & Pierce, D. W. (2017). Precipitation in a warming world: Assessing projected hydro-climate of California and other Mediterranean climate regions. *Nature Scientific Report*, *7*(1), 10783. https://doi.org/10.1038/s41598-017-11285-y

Polade, S. D., Pierce, D. W., Cayan, D. R., Gershunov, A., & Dettinger, M. D. (2014). The key role of dry days in changing regional climate and precipitation regimes. *Nature Scientific Report*, *4*, 4364.

Rayner, N. A., Parker, D. E., Horton, E. B., Folland, C. K., Alexander, L. V., Rowell, D. P., et al. (2003). Global analyses of sea surface temperature, sea ice, and night marine air temperature since the late nineteenth century. *Journal of Geophysical Research*, *108*(D14), 4407. https://doi.org/10.1029/2002JD002670

Rossby, C. G. (1940). Planetary flow patterns in the atmosphere. *Quarterly Journal of the Royal Meteorological Society*, *66*, 68–87.

Rutz, J. J., & Steenburgh, W. J. (2012). Quantifying the role of atmospheric rivers in the interior western United States. *Atmospheric Science Letters*, *13*(4), 257–261. https://doi.org/10.1002/asl.392

Rutz, J. J., Steenburgh, W. J., & Ralph, F. M. (2014). Climatological characteristics of atmospheric rivers and their inland penetration over the western United States. *Monthly Weather Review*, *142*(2), 905–921. https://doi.org/10.1175/MWR-D-13-00168.1

Sawyer, J. S. (1965). Notes on the possible physical causes of long-term weather anomalies, WMO technical note no. *World Meteorological Organization*, *66*, 227–248.

Scaife, A. A., Comer, R. E., Dunstone, N. J., Knight, J. R., Smith, D. M., MacLachlan, C., et al. (2017). Tropical rainfall, Rossby waves and regional winter climate predictions. *Quarterly Journal of the Royal Meteorological Society*, *143*(702), 1–11. https://doi.org/10.1002/qj.2910

Scanlon, B. R., Faunt, C. C., Longuevergne, L., Reedy, R. C., Alley, W. M., McGuire, V. L., & McMahon, P. B. (2012a). Groundwater depletion and sustainability of irrigation in the US High Plains and Central Valley. *Proceedings of the National Academy of Sciences*, *109*(24), 9320–9325. https://doi.org/10.1073/pnas.1200311109

Schanze, J. J., Schmitt, R. W., & Yu, L. L. (2010). The global oceanic freshwater cycle: A state-of-the-art quantification. *Journal of Marine Research*, *68*(3), 569–595. https://doi.org/10.1357/002224010794657164

Schmitt, R. W. (1995). The ocean component of the global water cycle. *Reviews of Geophysics*, *33*(S2), 1395–1409. https://doi.org/10.1029/95RG00184

Schwarz, G. E. (1978). Estimating the dimension of a model. *The Annals of Statistics*, *6*(2), 461–464. https://doi.org/10.1214/aos/1176344136

Seager, R., Naik, N., & Vecchi, G. A. (2010). Thermodynamic and dynamic mechanisms for large-scale changes in the hydrological cycle in response to global warming. *Journal of Climate*, *23*(17), 4651–4668. https://doi.org/10.1175/2010JCLI3655.1

Sharma, A., Luk, K. C., Cordery, I., & Lall, U. (2000). Seasonal to interannual rainfall probabilistic forecasts for improved water supply management: Part 2—Predictor identification of quarterly rainfall using ocean-atmosphere information. *Journal of Hydrology*, *239*(1-4), 240–248. https://doi.org/10.1016/S0022-1694(00)00347-4

Shields, C. A., & Kiehl, J. T. (2016). Atmospheric river landfall-latitude changes in future climate simulations. *Geophysical Research Letters*, *43*, 8775–8782. https://doi.org/10.1002/2016GL070470

Swain, D. L. (2015). A tale of two California droughts: Lessons amidst record warmth and dryness in a region of complex physical and human geography. *Geophysical Research Letters*, *42*, 9999–10,003. https://doi.org/10.1002/2015GL066628

Swain, D. L., Horton, D. E., Singh, D., & Diffenbaugh, N. S. (2016). Trends in atmospheric patterns conducive to seasonal precipitation and temperature extremes in California. *Science Advances*, *2*(4), e1501344. https://doi.org/10.1126/sciadv.1501344

Teng, H., & Branstator, G. (2016). Causes of extreme ridges that induce California droughts. *Journal of Climate*, *30*, 1477–1492.

Tseng, Y.-H., Ding, R., & Huang, X.-M. (2017). The warm blob in the Northeast Pacific—The bridge leading to the 2015/16 El Niño. *Environmental Research Letters*, *12*(5), 054019. https://doi.org/10.1088/1748-9326/aa67c3

Wang, S.-Y., Yoon, J.-H., Becker, E., & Gilles, R. (2017). California from drought to deluge. *Nature Climate Change*, *7*(7), 465–468. https://doi.org/10.1038/nclimate3330

Westerling, A. L., Hidalgo, H. G., Cayan, D. R., & Swetnam, T. W. (2006). Warming and earlier spring increase western U.S. forest wildfire activity. *Science*, *313*(5789), 940–943. https://doi.org/10.1126/science.1128834

Zeng, L., Chassignet, E., Schmitt, R. W., Xu, X., & Wang, D. (2018). Salinification in the South China Sea since late 2012: A reversal of the freshening since 1990s. *Geophysical Research Letters*, *45*, 2744–2751. https://doi.org/10.1002/2017GL076574

Zhang, R., & Delworth, T. L. (2006). Impact of Atlantic Multidecadal Oscillations on India/Sahel rainfall and Atlantic hurricanes. *Geophysical Research Letters*, *33*, L17712. https://doi.org/10.1029/2006GL026267

Zhang, Y., Wallace, J. M., & Battisti, D. S. (1997). ENSO-like interdecadal variability: 1900-93. *Journal of Climate*, *10*(5), 1004–1020. https://doi.org/10.1175/1520-0442(1997)010<1004:ELIV>2.0.CO;2

Zhu, Y., & Newell, R. E. (1998). A proposed algorithm for moisture fluxes from atmospheric rivers. *Monthly Weather Review*, *126*(3), 725–735. https://doi.org/10.1175/1520-0493(1998)126<0725:APAFMF>2.0.CO;2